# Direct Observation and Image-Based Simulation of Three-Dimensional Tortuous Crack Evolution inside Opaque Materials

Lihe Qian,[1,*] Hiroyuki Toda,[1] Kentaro Uesugi,[2] Masakazu Kobayashi,[1] and Toshiro Kobayashi[1]

[1]*Department of Production Systems Engineering, Toyohashi University of Technology, Toyohashi, Aichi, 441-8580, Japan*

[2]*Japan Synchrotron Radiation Research Institute, Sayo, Hyogo, 679-5198, Japan*

(Received 17 August 2007; published 21 March 2008)

We present a combined novel methodology to study the three-dimensional complex geometry of a tortuous crack and identify the essential features of the crack and its propagation inside a heterogeneous material. We find that some severe damage events occur unexpectedly below a local mode-I crack within the sample; we realize that the severe plastic zone of the local mode-I crack is shifted down by another unseen crack segment hidden behind, which is responsible for the unusual damage phenomenon observed. We also find that the crack grows fast at some locations but slowly at some other locations along the crack front; we recognize that the crack-tip fields are reduced by neighboring hidden crack segments, which accounts for the retarded propagation of some part of the crack front. The feasibility and power of the proposed methodology highlights the potential of a new way to study fracture mechanisms in real materials.

DOI: 10.1103/PhysRevLett.100.115505 PACS numbers: 62.20.M−, 62.20.F−

A complete understanding of fracture mechanisms in materials is necessary to improve their fracture resistance and reliability, which is essential for both science and industries [1]. *In situ* surface observations are often used to examine fracture processes for an interpretation of the underlying mechanisms. However, these observations do not provide bulk information on damage inside opaque materials [2,3]. This is because heterogeneities are existent in real materials, and the stress-strain state on the viewing surface differs from that in the interior, both of which tend to cause a different behavior observed on the surface and inside the materials. An alternative way is to apply a sectioning technique, by which the internal damage can be examined after loading [4]. This method can assist in analyzing the damage-microstructure interactions within the sample, but does not allow following the dynamics of the damage process due to its destructiveness. Fortunately, the aforementioned deficiencies can now be overcome by synchrotron x-ray computed tomography (CT). CT has recently been applied to study the internal microstructure of materials [5–7] and to assess three-dimensional (3D) crack and fracture behavior as well [8,9], which suggests the potential of its application in micromechanical understanding of fracture mechanisms in three dimensions.

Moreover, analytical models or numerical simulations are also used to understand fracture behavior. Various crack-oriented models have been proposed and applied, and they are capable of predicting stress or strain fields and damage events in materials [10,11]. Almost all of these models deal with a homogeneous medium, and assume straight, flat crack geometry and/or a plane stress or strain state, and thus, relatively simplified crack-tip fields often result from such simplifications. Nevertheless, real materials are inhomogeneous, crack surface is nonplanar, crack front is torturous, and crack-crack interactions are existent as well in the presence of multiple cracks [6–8]. Therefore, deformation fields near the front of a 3D crack with complex morphology can be very complicated. Consequently, while considerable effort has been devoted to the modelling work, and the models do provide general knowledge of deformation and damage, they are unable to accurately capture local-scale damage events and crack evolution behavior in a cracked medium of a real material. Accordingly, only a 3D model that takes into account real crack morphology is expected to identify all key features of fracture that involves the evolution of local stress or strain fields [3,12]. Furthermore, a realistic validation of the modelling results needs 3D experimental verification, i.e., the knowledge of real 3D crack evolution behavior. However, such actual modelling of real crack problems along with realistic experimental verification has not become feasible until now [13–15]. Here, we apply a high-resolution x-ray CT technique (that allows *in situ* watching the propagation of a 3D crack inside opaque materials during loading) combined with an image-based simulation (that takes into account actual 3D crack geometry) to study a real tortuous crack and its propagation behavior inside a real heterogeneous material.

The material selected was a model Al-7Si-1Mg alloy, which consists of a $\alpha$ phase (an Al-based solution) and a eutectic phase (an Al matrix dispersed with eutectic Si particles). Parallelepiped tensile specimens with a single-edged precrack were prepared for the *in situ* tomography experiment. The specimens were required to be small enough to fit the field of view for obtaining a high-resolution tomography image at a micron level. To do so, a three-point bend sample [of a size $10 \times 10 \times 50$ $(\mathrm{mm})^3$] with a cutting notch was first prepared. A fatigue crack was then produced using a load-decreasing method. The desired tensile specimens, having a cross section of $0.6 \times 0.6$ $(\mathrm{mm})^2$ and a precrack length of 0.25 mm, were finally cut from the crack-tip region of the fatigued sample. The experiment was performed at the Japanese third-generation synchrotron radiation facility, Spring-8. A test rig, which

 

had been specially designed for the x-ray tomography, was used [9]. High-resolution x-ray tomography was performed during tensile loading. Seven tomography scans were made, which corresponded to different loading steps. (The increments of the applied displacement for the field of view corresponding to steps $1 \sim 7$ are 0, 1.9, 5.7, 9.5, 14, 29, and 53 $\mu$m, respectively). The reconstructed slice images were stacked and rendered to produce 3D images with an isotropic voxel size of $(0.47\ \mu\text{m})^3$ using a commercial visualization software. The crack, damage and microstructure were examined in detail within small volumes of choice and on virtual slices of interest. Additionally, different components in the 3D image were extracted by segmentation technique to capture the features of the components and their evolution behavior.

Three-dimensional image-based finite-element simulations were performed for a better understanding of the observed phenomena. The model consists of a uniform Al-7Si-1Mg alloy embedded with a real complicated 3D crack as illustrated in Fig. 1, and contains a total number of ~126 000 tetrahedral elements. A commercial finite-element analysis program was used for the simulations. A static loading was applied until an applied displacement of 14 $\mu$m, which corresponds to loading step 5 in the *in situ* experiment. No attempt was made to simulate crack growth at the moment.

The reconstructed 3D rendering of the unloaded microstructure together with the initial precrack in the sample is shown in Fig. 2(a); the extracted complex geometry of the entire crack is illustrated in Fig. 2(b). One key feature of the crack before its propagation is that, over a range of ~180 $\mu$m behind the crack front, the crack is divided into three segments I, II, and III in the width direction [$z$ axis, Fig. 2(b)]. The three segments lie on different horizontal planes and overlap each other slightly between the neighboring ones. The front line of each crack segment is tortuous, and the surfaces of the entire crack are rough. The evolution process of the 3D crack is presented in Fig. 2(c)–2(e). The crack was opened and voids were initiated within the sample with loading [Fig. 2(c)]; and no obvious crack propagation occurred until an applied displacement of 14 $\mu$m. With further loading, some voids grew and connected, which caused the propagation of the main crack [Fig. 2(d) and 2(e)]. Near the side surfaces of the sample, the crack remained nearly nonpropagated up to the applied maximum displacement of 53 $\mu$m. However, in the interior, the growth amount and direction of the crack varied from location to location along the crack front. The retarded propagation of the crack on the side surfaces may

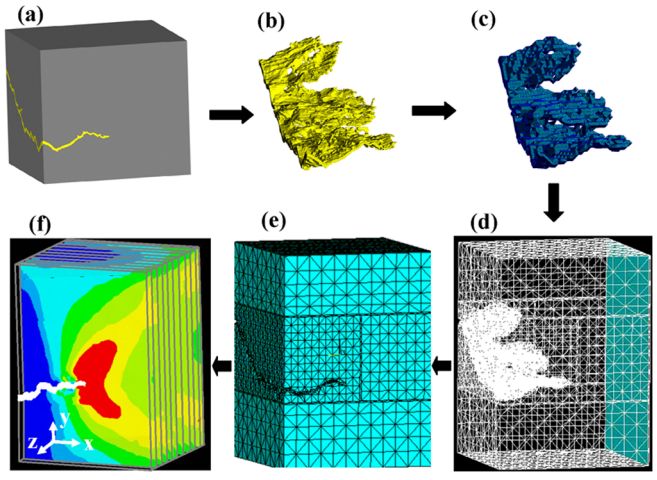


FIG. 1 (color online). Flow chart of creating image-based crack model. (a) 3D image of microstructure containing a complicated crack. (b) Crack volume segmented by thresholding the gray value from the 3D image data. (c) Crack surface extracted by tracing the iso-gray-value surfaces with triangular surface meshes. (d) and (e) Constructed 3D model. (f) Simulated equivalent stress contour pattern.

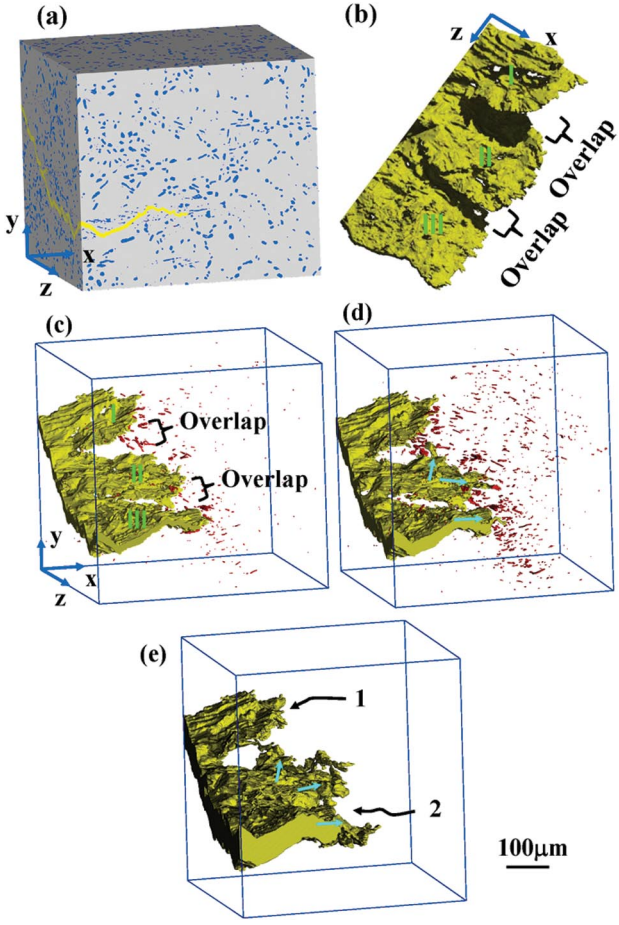


FIG. 2 (color). Three-dimensional rendering of (a) the microstructure (aluminum in gray, particles in blue) and crack (yellow) before loading was applied; and (b)–(e) the crack and voids (red) in the entire volume at loading steps 3, 5, 6, and 7, respectively. The loading is in $y$ direction. I, II, and III indicate three crack segments. The blue straight arrows indicate where crack grows largely, while arrows 1 and 2 indicate where crack has not grown yet. Note that voids are made invisible in (b) and (e) for clarity.

be due to the fact that the local crack driving force, which governs the intensity of near-tip fields and thus the void-initiated damage, decreases as the free surfaces are approached [16]. On the other hand, the reason for a wide variation of crack growth amount and direction along the 3D crack front may be attributable to the heterogeneities in the material; however, other factors, which are likely to be existent but hidden, may be also responsible.

Closer examinations revealed many more essential features of fracture, as typically shown in Fig. 3(a)–3(c). An extracted subvolume ranging from $z = 0$ to 80 $\mu$m is shown in Fig. 3(a). In this subvolume, crack segments I and II are partially overlapped. We find that the voids were initiated in the vicinity of the crack front, but almost entirely between the two crack segments. This phenomenon may result from the interactions between the two crack segments. An even smaller subvolume extracted from the volume in Fig. 3(a), ranging from $z = 0$ to 50 $\mu$m, is shown in Fig. 3(b). Crack segment I only is existent. The crack front region is almost planar and vertical to the loading direction ($y$ axis). This is typical of a mode-I crack, although it is slanted in the wake zone. We find that the voids were initiated primarily below crack segment I, with the damage zone (sketched out by the dashed line) shifted downwards. This phenomenon is, however, inconsistent with usual anticipation that the initiation and growth of voids should occur in a kidney-shape region centered at the crack front, corresponding to the theoretically predicted plastic zone of a mode-I crack. One may argue that this unusual phenomenon may be caused by a nonuniform distribution of particles, since clustered particles are known to be more easily damaged than uniform ones [17]. We examined this possibility, and found that particles are indeed nonuniformly distributed; however, we did not find evidence that the region corresponding to the severely-damaged zone is more clustered than other regions [Fig. 3(c)]. This implies that the effect of particle distribution may not be the major reason for the down-shifted damage zone observed in Fig. 3(b). And thus, the actual operative mechanisms need to be identified further.

We investigated the stress and strain fields on various cross sections of the image-based crack model. Two typical plots of plastic-strain contour patterns are demonstrated in Fig. 3(d) and 3(e), side by side with the aforementioned experimental observations in Fig. 3(a) and 3(b). Crack segment I is overlapped with crack segment II in Fig. 3(d), which corresponds to the front cross section of the volume shown in Fig. 3(a). We find that the severe plastic zone occurs, interestingly, between the upper and lower cracks. This agrees very well with the damage zone observed in the *in situ* experiment [as dashed out in Fig. 3(a)]. We may suppose that such a contour pattern is a superimposed result of the overlapped crack segments I and II, which affect each other in the overlapped region. In contrast, however, crack segment I only (which is a mode-I crack) is present in Fig. 3(e), which corresponds to the front cross section of the volume shown in Fig. 3(b). We find that the severe plastic zone lies below the tip of crack segment I and the outer strain contours are centered on a dashed straight line beneath the crack tip [Fig. 3(e)]. Although this contour pattern matches so well with the observed down-shifted damage zone in Fig. 3(b), it is not expected from a single mode-I crack in Fig. 3(e). On the other hand, we can assume that the stress or strain fields and as well the severe plastic zone of crack segment I in Fig. 3(e) may have been affected by the neighboring crack

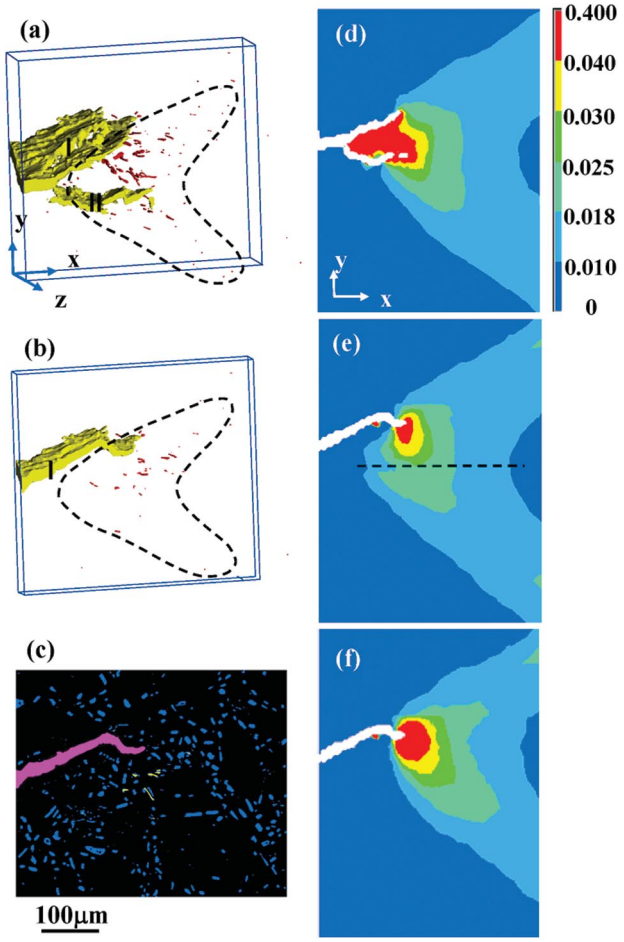


FIG. 3 (color). (a) A subvolume (ranging from $z = 0$ to 80 $\mu$m) extracted from the entire crack volume; and (b) a smaller subvolume (ranging from $z = 0$ to 50 $\mu$m) extracted from that in (a). Aluminium and particles are made invisible to highlight the crack (yellow) and voids (red). (c) A cross sectional image of microstructure at $z = 50$ $\mu$m, which corresponds to the front cross section in (b), showing the interactions among the crack (pink), particles (blue), and voids (yellow). All the images correspond to loading step 5. Equivalent plastic-strain contours on the cross sections of (d) $z = 80$ $\mu$m and (e) $z = 50$ $\mu$m. (f) Equivalent plastic-strain contours of the same cross section as in (e), but obtained from the control simulation in which crack segment II was not included. All the contours correspond to loading step 4.

segment II existent in Fig. 3(d), even though they are not overlapped in Fig. 3(e). This assumption is due to the fact that the two cross sections in Fig. 3(d) and 3(e) are spatially close to each other, with only 30 $\mu$m apart on $z$ axis.

To further confirm the above assumption, we made a control simulation using the same model, but crack segment II was removed, and thus, its potential effect was ruled out. The plastic-strain contours of the same cross section as in Fig. 3(e) (but obtained from the control simulation) is shown in Fig. 3(f). We find that the contour pattern in Fig. 3(f) approaches to that of a mode-I crack with the severe plastic zone and near-tip contours centered at the crack tip, which is obviously different from that in Fig. 3(e). This observation indicates that the existence of crack segment II does change the stress or strain fields of crack segment I and shift its severe plastic zone, even in the case of nonoverlapping. From Fig. 3(f), we can also find that the intensity of near-tip plastic deformation is increased and the size of severe plastic zone is enlarged as well, when compared with Fig. 3(e). This finding indicates that when crack segment II is present, not only the severe plastic zone of crack segment I is shifted, but also the magnitude of its near-tip stress or strain fields is reduced, even on the cross section where crack segment II is unseen [Fig. 3(e)]. Such a stress shielding effect should be one major reason for the retarded propagation of the crack front near the overlapped regions (e.g. arrows 1 and 2, Fig. 2).

The combined methodology of *in situ* 3D crack visualization and image-based crack simulation has been demonstrated to be powerful and feasible in revealing and understanding various fracture phenomena inside materials. Using this methodology, many essential features of crack and crack propagation behavior have been identified three-dimensionally in this Letter. Typically, we have recognized that one crack segment affects significantly the fracture behavior of another neighboring hidden crack segment by shielding the near-tip stress or strain fields and shifting the near-tip plastic zone of the crack in the studied sample. We can expect that different interactions between crack segments may be existent in other samples, which depend on the morphologies of individual crack segments. We know that crack-crack interactions between crack branches or flat parallel cracks, which overlap each other and penetrate through specimen thickness thus being visible on any one observation surface, have been extensively studied [18–21]. However, the interactions between nonoverlapped crack segments have neither been noticed nor investigated previously, because these crack segments do not appear on the same cross sections thus being inaccessible to traditional surface based imaging techniques. The findings made in this work are remarkable, since surface observations only may lead to misunderstanding of operative damage mechanisms, without considering the 3D effects of microstructure and crack such as the interactions between possibly existent nonoverlapped crack segments. We anticipate this work as a starting point to be extended further for a better understanding of the underlying mechanisms of fracture in various materials. And hence, some new insight into materials fracture behavior may be available, and some definite answers to crack problems that have been puzzling material researchers would therefore finally be at hand.

We thank the Grant-in-aid for Scientific Research from JSPS through subject No. 16-04370. The synchrotron radiation experiment was performed at the Spring-8 with the approval of JASRI.

*Corresponding author: dlhqian@yahoo.com

[1] J. Kierfeld and V. M. Vinokur, Phys. Rev. Lett. **96**, 175502 (2006).
[2] K. B. Broberg, *Cracks and Fracture* (Academic Press, New York, 1999).
[3] M. Heyder and G. Kuhn, International Journal of Fatigue **28**, 627 (2006).
[4] A. Ayyar and N. Chawla, Compos. Sci. Technol. **66**, 1980 (2006).
[5] B. P. Flannery, H. W. Deckman, W. G. Roberge, and K. L. D'Amico, Science **237**, 1439 (1987).
[6] A. Kulkarni *et al.*, Metall. Mater. Trans. A **35**, 1945 (2004).
[7] L. Babout, E. Maire, J.-Y. Buffiere, and R. Fougeres, Acta Mater. **49**, 2055 (2001).
[8] H. Toda *et al.*, Acta Mater. **52**, 1305 (2004).
[9] L. Qian *et al.*, Appl. Phys. Lett. **87**, 241907 (2005).
[10] R. M. McMeeking and D. M. Parks (ASTM STP 668, Philadephia, 1979), p. 175.
[11] S. Suresh and C. F. Shih, Int. J. Fract. **30**, 237 (1986).
[12] Y. Fang, T. Fossier, and K. W. White, Scr. Mater. **50**, 127 (2004).
[13] J. Wulf, T. Steinkopff, and H. F. Fischmeister, Acta Mater. **44**, 1765 (1996).
[14] Z. Shan and A. M. Gokhale, Int. J. Plast. **20**, 1347 (2004).
[15] B. Cox and Q. Yang, Science **314**, 1102 (2006).
[16] T. Nakamura and D. M. Parks, J. Mech. Phys. Solids **38**, 787 (1990).
[17] S. Ghosh and S. Moorthy, Acta Mater. **46**, 965 (1998).
[18] S. V. Kamat and J. P. Hirth, Acta Mater. **44**, 1047 (1996).
[19] X. B. Zhang, S. Ma, N. Recho, and J. Li, Eng. Fract. Mech. **73**, 1925 (2006).
[20] M. Isida, K. Hirota, H. Noguchi, and T. Yoshida, Int. J. Fract. **27**, 31 (1985).
[21] Y. Murakami and S. Nemat-Nasser, Eng. Fract. Mech. **16**, 373 (1982).